Title page

Lineage Analysis and Molecular Characterization of Bergmann Glia-like Progenitors in the Postnatal Mouse Cerebellum using *in vivo* Electroporation and Spatial Transcriptomics

Author names

Kyoka Suyama[1, 2, 4], Toma Adachi[1, 4, *], Eriko Isogai[1], Ikuko Hasegawa[1], Minami Mizuno[1, 3], Ji Kaiyuan[1, 2], Kayo Nishitani[1] Satoshi Miyashita[1], Tomoo Owa[1], Mikio Hoshino[1, *]

Affiliations

[1]Department of Biochemistry and Cellular Biology, National Center of Neurology and Psychiatry (NCNP), Tokyo 187-8502, Japan

[2]Graduate School of Medical and Dental Sciences, Science Tokyo, Tokyo 152-8550, Japan

[3]Department of Biomolecular Science, Graduate School of Science, Toho University, Chiba 274-8510, Japan

[4]These authors contributed equally

Corresponding author

*Correspondence: toma.adachi@ncnp.go.jp (T.A.), hoshino@ncnp.go.jp (M.H.)

Keywords

Cerebellum, Astroglial cell, Bergmann glia-like progenitor, *in vivo* electroporation, spatial transcriptomics

Short title

Lineage and Molecular Profiling of Bergmann Glia-like Progenitors in Postnatal Mouse Cerebellum

Abstract

Astroglial cell diversity is essential for proper brain development and function in mammals. In mammalian cerebellum, three types of astroglial cells—Bergmann glial cells (BGs), inner granule cell layer (IGL) astrocytes, and white matter (WM) astrocytes—arise in postnatal timing from two types of progenitors: Bergmann glia-like progenitors (BGLPs) and astrocyte-like progenitors (AsLPs). While BGLPs are known to differentiate into BGs and IGL astrocytes in postnatal day 6 (P6) mice,

their fate immediately after birth remains unclear due to technical challenges in specifically labeling BGLPs. In this study, we demonstrated that both BGLPs and AsLPs gradually decrease from P0 to P10. Using *in vivo* electroporation to label BGLPs, we found that BGLPs in P0 mice differentiate not only into BGs, IGL astrocytes but also WM astrocytes. Using spatial transcriptomics analysis (Xenium, 5k), we achieved the isolation and comparative profiling of BGLP clusters from P0 and P6 mice. This analysis revealed that P0 BGLPs exhibit more stem cell-like features, while P6 BGLPs show a shift toward BG-like characteristics. These findings indicate that BGLPs immediately after birth possess higher pluripotency than previously recognized.

Introduction

The diversity of astroglial cells plays a crucial role in normal brain development and function in mammals (Vivi *et al*., 2024, Khakh *et al*., 2015). In the cerebellum of adult mammals, three types of astroglial cells are found: astrocytes with a multipolar morphology located in the inner granule cell layer (IGL) and white matter (WM)—referred to as IGL astrocytes and WM astrocytes, respectively—and Bergmann glial cells (BGs), which have a unipolar morphology, with their cell bodies in the Purkinje cell layer (PCL) and long processes extending to the pia mater (Leto *et al*., 2016). In the cerebellum of postnatal mice, astroglial cells are produced from two types of progenitors. One of these is Bergmann glia-like progenitors (BGLPs) which have a similar morphology and localization to BGs. The other is astrocyte-like progenitors (AsLPs) which have a multipolar morphology and are localized in the WM. These progenitors are thought to be present until approximately one week after birth, but the exact postnatal stage at which they disappear is unknown.

BGLPs of postnatal day 6 (P6) mice are known to differentiate into BGs and IGL astrocytes (Joyner & Bayin, 2022; Cerrato *et al*., 2018). Moreover, in the cerebellum, when granule cell progenitors (GCPs) are depleted by irradiation immediately after birth, BGLPs have been shown to transdifferentiate and compensate for the loss of GCPs (Bayin *et al*., 2021). Although BGLPs have such high pluripotency, it remains unclear into which cell types they differentiate under normal

conditions at earlier postnatal stages, particularly immediately after birth (P0). This uncertainty is partly because labeling only BGLPs and not AsLPs in P0 mice, and then analyzing the lineage, are technically challenging.

In this study, we first demonstrated that both types of astroglial progenitors, BGLPs and AsLPs, gradually decreased from P0 to P10 and were nearly absent by P10. Using *in vivo* electroporation (EP) labeling BGLPs, we further revealed that BGLPs in P0 mice differentiate not only into BGs and IGL astrocytes but also into WM astrocytes. Additionally, through spatial transcriptomics analysis (Xenium 5k), we achieved the first successful isolation of BGLPs in P0 and P6 mice by unsupervised clustering. Comparative analysis of their gene expression profiles showed that BGLPs at P0 exhibited more stem cell-like characteristics, whereas BGLPs at P6 displayed stronger BG-like features. These findings suggest that BGLPs immediately after birth possess higher pluripotency than previously recognized.

Results

BGLPs and AsLPs are present in the postnatal mouse cerebellum until P10

BGLPs and AsLPs are astroglial progenitors that remain in the cerebellum of postnatal mice. However, the precise timing of their persistence remains unclear. Therefore, we first measured the changes in the number of the two types of astroglial progenitors at each postnatal stage (Fig. 1a, b). We sectioned the midline vermis region sagittally. Astroglial lineage cell (astroglial progenitors and astroglial cells) nuclei were stained with SOX9 antibody and the cellular shapes were visualized with either VIMENTIN (P0-P4) or GFAP (P6-P21) antibodies. BGLPs are SOX9+ and KI67+ cells that localize in the PCL and have unipolar projections extending toward the pia. AsLPs are SOX9+ and KI67+ cells that localize in deeper layers than PCL with a multipolar morphology. We counted the number of BGLPs and AsLPs in each mouse stage. We found that the number of BGLPs and AsLPs gradually decreased from P0 to P10, and that both were nearly absent at P10 (Fig. 1a, b). We also measured the number of BGs and astrocytes and observed that the number of BGs and astrocytes

increased rapidly from P0 to P10 (Fig. 1a, c). After P10, no further increase was observed (Fig. 1c). These results indicate that astroglial cells increase in number during the period up to P10, when astroglial progenitors are still detectable. These findings further support previous studies that BGs and astrocytes are derived from BGLPs and AsLPs in the postnatal mouse cerebellum (Joyner & Bayin, 2022).

Electroporation method labels BGLPs at P0 and P6

To date, it has remained unclear which cell types are generated from BGLPs in mice immediately after birth (P0). One reason for this is that it was technically challenging to label only BGLPs and not AsLPs in P0 mice, and then analyze the lineage. Previously, we established a method for introducing DNA vectors into GCPs using the EP method (Adachi *et al*., 2021; Miyashita *et al*., 2021; Yamashita *et al*., 2020; Owa *et al*., 2018). Furthermore, we confirmed that this technique introduced vectors not only into GCPs but also a few SOX9+ cells (astroglial lineage cells) in P1 mice (Owa *et al*., 2018). However, it was not known which type of SOX9+ cells (astroglial lineage cells) were labeled by this EP method. Therefore, we hypothesized that BGLPs in P0 mice could be labeled using this EP method. Thus, we electroporated a CAG-driven mCherry vector (CAG-mCherry) into the P0 mouse cerebellum (Fig. 2a-h). Then, by fixing the brain one day after EP, we identified the cell type into which the vector was introduced. As a result, approximately 20 cells per cerebellar lobule were labeled by mCherry (18.769 ± 1.553, Fig. 2a, e). We found that approximately 10% of these mCherry+ cells were BG-like cells (PCL localized astroglial cells with unipolar processes, BGLPs or BGs) (0.118 ± 0.021, Fig. 2d, f), and approximately 90% were GC lineage cells (GCPs and GCs) localizing in the external granule cell layer (EGL) (0.928 ± 0.003, Fig. 2a, f). We did not detect mCherry signals in the other cell types in the cerebellum (Fig. 2a, b, c, f). Furthermore, we observed that approximately half of the mCherry+ BG-like cells were BGLPs (0.545 ± 0.039, Fig. 2g, h). We also found that the method did not label multipolar AsLPs or astrocytes that were localized in deeper

layers than PCL (Fig. 2f). GCPs are neuronal progenitors known not to differentiate into astroglial cells (Vladoiu *et al.*, 2019; Machold ＆ Fishell, 2005). Based on these findings, we concluded that, when the vector was introduced at P0, the mCherry+ astroglial cells after the EP were either descendants of BGLPs or cells that were already BG at the time of EP.

Previously, a lineage-tracing experiment revealed that BGLPs in P6 mice differentiate into BGs and IGL astrocytes (Cerrato *et al.*, 2018). To evaluate whether our *in vivo* EP method could reproduce this finding, we performed EP using the CAG-mCherry vector in the P6 cerebellum and fixed the tissue at P7 (Fig. 2i-p). As a result, there were approximately 30 mCherry+ cells per lobule (28.554 ± 2.728, Fig. 2i, m). Among them, approximately 5% were BG-like cells (0.063 ± 0.006, Fig. 2l, n), and 95% were EGL-localizing GC lineage cells (0.953 ± 0.005, Fig. 2i, n). Even under P6 EP conditions, we did not observe mCherry signals in other cell types in the cerebellum (Fig. 2i, j, k, n). Furthermore, approximately 30% of the mCherry+ BG-like cells were BGLPs (0.286 ± 0.067, Fig. 2o, p). We also found that the method did not label multipolar AsLPs or astrocytes that were localized in layers deeper than the PCL (Fig. 2n). Based on these findings, we concluded that even when the vector was introduced at P6, the mCherry+ astroglial cells after EP were either descendants of BGLPs or cells that were already BG at the time of EP. These results suggest that the EP method is a useful tool for labeling BGLPs and performing lineage analysis in P0 and P6 mice.

<u>BGLPs at P0, but not at P6, differentiate into WM-localized astrocytes at P10</u>

To analyze the lineage of BGLPs, we introduced CAG-mCherry into the P0 and P6 mouse cerebellum using the EP method and fixed them at P10, when BGLPs were no longer present (Fig. 3a, b). When the vector was introduced at P0, the number of astroglial cells labeled with mCherry was approximately six per lobule (6.347 ± 0.741) and approximately two at P6 (1.787 ± 0.345, Fig. 3b, c). In addition, among the mCherry+ cells, the proportion of astroglial cells was approximately 54% when the vector was introduced at P0 (0.544 ± 0.054) and approximately 8% when introduced at P6 (0.077

± 0.018, Fig. 3b, d). Furthermore, we investigated the distribution of the labeled astroglial cells. We found that when the vector was introduced at P0, in addition to the BGs and IGL-localized astrocytes, WM-localized astrocytes were labeled with mCherry (WM-localized astrocyte ratio: 0.327±0.023, Fig. 3b, e). In contrast, when we introduced the vector at P6, only BGs and IGL-localized astrocytes were labeled with mCherry (WM-localized astrocyte ratio: 0.011 ± 0.010; Fig. 3b, e). These findings indicate that BGLPs at P0 differentiate into BGs, IGL-localized astrocytes, and WM-localized astrocytes, whereas BGLPs at P6 give rise exclusively to BGs and IGL-localized astrocytes.

BGLPs at P0, but not at P6, differentiate into WM astrocytes in the mature cerebellum

The results suggest that BGLPs in P0 mice produce not only BGs and IGL-localized astrocytes, but also WM-localized astrocytes, which differ from those in P6 mice. However, the cerebellum of P10 mice is still developing, and astroglial cells observed at P10 may subsequently migrate to other layers. Therefore, to examine the differentiation state of mCherry+ astroglial cells in the fully developed cerebellum, we introduced the CAG-mCherry vector into the cerebellum of P0 and P6 mice using EP and observed them at P30 (Fig. 4a, b). As a result, when the vector was introduced at P0, the number of astroglial cells labeled with mCherry was four per lobule (4.438 ± 0.737), and approximately three at P6 (3.435 ± 0.593, Fig. 4b, c). In addition, among the mCherry+ cells, the proportion of astroglial cells was approximately 45% when the vector was introduced at P0 (0.445 ± 0.072) and 12% at P6 (0.123 ± 0.017, Fig. 4b, d). The results obtained at P30 were not significantly different from those at P10 (Fig. 4c, d). We also investigated the distribution of mCherry+ astroglial cells. We found that when the vector was introduced at P0, there were WM astrocytes in addition to BGs and IGL astrocytes, as observed at P10 (WM astrocyte ratio: 0.297±0.031, Fig. 4b, e). In contrast, when we introduced the vector at P6, we found that only the BGs and IGL astrocytes were labeled with mCherry (WM astrocyte ratio: 0.011±0.010, Fig. 4b, e). No significant differences were observed when comparing the proportion of each astroglial cell type between the two different fixation times,

P10 and P30 (Fig. 4f). These results suggest that BGLPs in P0 mice differentiate not only into BGs and IGL astrocytes but also into WM astrocytes in the fully developed cerebellum, whereas BGLPs in P6 mice differentiate only into BGs and IGL astrocytes. P6 experimental results were consistent with those of a previous lineage tracing study using genetically modified mice (Cerrato *et al*., 2018). These results suggest that BGLPs in P0 mice were more pluripotent than those in P6 mice and produced WM astrocytes.

Introduction of the hGFAP-eGFP vector via the electroporation method specifically labels BGLPs at P0

We then attempted to develop a method for labeling only BGLPs using EP. The hGFAP promoter is known to promote gene transcription specifically in astroglial progenitors and astroglial cells in the postnatal cerebellum (Zhuo *et al*., 1997). Therefore, we decided to perform EP using a vector in which eGFP transcription was driven by the hGFAP promoter (hGFAP-eGFP). We co-electroplated hGFAP-eGFP and CAG-mCherry vectors into the cerebellum of P0 mice. Then, by fixing the cerebellum one day after EP, we investigated which cells were labeled with eGFP (Fig. 5). As a result, 1–2 cells per lobule were labeled with eGFP (1.354 ± 0.146, Fig. 5b, e), and 95% of these eGFP+ cells were BG-like cells (BGLPs and BGs) (0.948 ± 0.033, Fig. 5b, f). Furthermore, 93% of the labeled BG-like cells were BGLPs (KI67+) (0.933 ± 0.042, Fig. 5c, g). The cells labeled with eGFP were localized in the PCL and did not express NEUROD1, indicating that they were not differentiated GCs (Fig. 5d). Among the cells labeled with CAG-mCherry (GCPs and astroglial lineage cells), approximately 9% were labeled with hGFAP-eGFP (only astroglial lineage cells) (0.094 ± 0.011; Fig. 5c and h).

Next, we introduced hGFAP-eGFP and CAG-mCherry into the P6 mouse cerebellum by EP and fixed the cerebellum one day after EP (Supplemental Fig. 1a). Interestingly, we observed that not only BG-like cells but also GC lineage cells localized in the EGL were labeled with eGFP

(Supplemental Fig. 1b, c, d). Approximately 20% of the cells labeled with eGFP were BG-like cells (BGLPs and BGs) (0.217±0.014, Supplemental Fig. 1b, d). These results indicate that BGLPs were specifically labeled in the EP using the hGFAP-eGFP vector, at least in P0 mice.

Specifically labeled BGLPs at P0 differentiate into BG, IGL-localized astrocytes and WM-localized astrocytes

Next, we attempted to identify the cells into which BGLPs differentiate using the hGFAP-eGFP vector. To achieve this, we introduced the hGFAP-eGFP and CAG-mCherry vectors into the P0 mouse cerebellum and fixed the cerebellum at P10 (Fig. 6a, b). As a result, approximately 4–5 astroglial cells were labeled with eGFP per cerebellar lobule (4.594 ± 0.421, Fig. 6b and c). Furthermore, the proportion of astroglial cells among eGFP+ cells was nearly 100% (0.994 ± 0.005, Fig. 6b and d). Next, we investigated the distribution of astroglial cells labeled with eGFP. We found that there were also WM-localized astrocytes, in addition to BG- and IGL-localized astrocytes, as was the case for CAG-mCherry vector introduction (WM-localized astrocyte ratio: 0.292±0.029, Fig. 6b, e). Among the cells labeled with CAG-mCherry, approximately 41% were labeled with hGFAP-eGFP (0.409 ± 0.050; Fig. 6b, f). We found that the BGLPs of P0 mice produced WM-localized astrocytes using vectors with two different promoters. These results strongly support our hypothesis that BGLPs at P0 are more pluripotent than those at P6 and produce not only BGs and IGL astrocytes but also WM astrocytes.

Spatial transcriptomics analysis reveals distinct molecular signatures of P0 and P6 BGLPs

To investigate the differences in the molecular properties of BGLPs at the two stages, we conducted spatial transcriptomics (Xenium, 5k) using cerebellar sections from P0 and P6 mice (Fig. 7). In total, 5,146 and 19,892 cells were segmented in the P0 and P6 mice cerebellar slices, respectively. We applied unsupervised clustering, which identified 24 unique clusters of cells that were shared by the two stages (Fig. 7a, b, Supplemental Fig. 2a). We annotated each cluster with the expression

profiles of cerebellar cell markers and spatial information (Fig. 7c, Supplemental Fig. 3). We found that clusters 6 (1,117 cells), 11 (820 cells), and 13 (607 cells) corresponded to P0 and P6 astroglial lineage cells. To further subdivide the astroglial lineage cells, we combined clusters 6, 11, and 13, and performed sub-clustering in an unsupervised manner and eventually obtained 10 sub-clusters (Fig. 7d, Supplemental Fig. 2b). Most of the cells in sub-clusters 0, 6, and 7 were derived from P0, while sub-clusters 1, 2, 3, 4, and 5 were from P6 (Supplemental Fig. 2b). Sub-clusters 8 and 9 were omitted from further analysis because of their small cell populations and dispersed localization (Supplemental Fig. 2c). Based on the expression profiles of known BG-like cell-specific markers (*Gdf10, Gria1, Sept4*) and proliferative markers (*Pcna, Mki67*), and spatial information, we found that sub-cluster 7 corresponded to BGLPs in P0 mouse (Fig. 7e, f, Supplemental Fig. 2d-h), while sub-cluster 1 and 4 corresponded to BGLPs in P6 mouse (Fig. 7e, g, Supplemental Fig. 2i-m).

Next, we compared the transcript levels between the BGLP sub-clusters of P0 (sub-cluster 7) and P6 (sub-cluster 1 and 4) (Fig. 8a). We found 224 genes that were significantly more highly expressed in the BGLP sub-cluster at P0 than at P6 (referred to as “upregulated genes in P0 BGLP”) and 87 genes that were significantly more highly expressed at P6 than at P0 (referred to as “upregulated genes in P6 BGLP”) (Average Log2 Fold Change > 1, p_val_adj < 0.05, Fig. 8a). We then performed GO analysis on these differentially expressed genes (DEGs) (Fig. 8b, d). Several GO categories for “upregulated genes in P0 BGLP” were related to cell cycle progression, such as “nuclear division,” “mitotic cell cycle phase transition,” and “mitotic nuclear division” (Fig. 8b). Among the genes involved in cell cycle progression, the “upregulated genes in P0 BGLP” included *Nes*, *Sox4*, and *Sox11*, which are also known as stem cell markers (Fig. 8c). In contrast, some GOs for “upregulated genes in P6 BGLP” implicated glial cell differentiation, such as “gliogenesis,” “glial cell differentiation,” and “astrocyte differentiation” (Fig. 8d). Among the genes involved in glial cell differentiation, the “upregulated genes in P6 BGLP” included BG-like cell-specific markers such as *Gdf10, Gria1, Tnc,* and *Sept4* (Fig. 8e). These findings suggest that BGLPs in P0 mouse exhibit more stem cell-like characteristics, whereas BGLPs in P6 mouse display stronger BG-like features. These results are

consistent with our *in vivo* observations, which indicate that BGLPs in P0 mice exhibit higher pluripotency than those in P6 mice and are capable of producing WM astrocytes (Fig. 8g).

Finally, we explored the upstream transcription factors (TFs) that potentially regulate the gene expressions of BGLPs at P0 and P6. We utilized Enrichr (Chen *et al*., 2013) to explore TFs that could act as upstream regulators of the "upregulated genes in P0 BGLP" and "upregulated genes in P6 BGLP" (referred to as "upstream candidates for P0 BGLP" and "upstream candidates for P6 BGLP," respectively, including the top five genes from the datasets contained in Enrichr, Table1). Among the "upstream candidates for P0 BGLP", the only gene included in the "upregulated genes in P0 BGLP" was *Foxm1* (Fig. 8f). Similarly, among the "upstream candidates for P6 BGLP", the only gene included in the "upregulated genes in P6 BGLP" was *Nfia* (Fig. 8g). These findings suggest that *Foxm1* and *Nfia* may be involved in regulating the gene expression profiles of BGLPs at P0 and P6, respectively (Fig. 8g).

Discussion

In this study, we developed a technique for labeling BGLPs in P0 and P6 mice using EP. We clarified that BGLPs in P0 mice differentiate into BGs, IGL, and WM astrocytes. We also found that BGLPs in the cerebellum of P6 mice produced only BGs and IGL astrocytes, as previously known (Joyner & Bayin, 2022; Cerrato *et al*., 2018). These findings indicate that BGLPs in newborn mice possess a higher level of pluripotency than previously recognized.

After introducing CAG-mCherry, we fixed the mouse cerebellum at P10 or P30. We found no significant differences in the number of mCherry+ astroglial cells or the percentage of each astroglial cell type (BG, IGL astrocyte, and WM astrocyte) between the two fixed times. These data suggest that after P10, when BGLPs disappeared, the astroglial cells generated from BGLPs did not increase in number or migrate from their respective layers. In a previous study, Mockenhaupt *et al*. performed single-cell RNA sequencing (sc-RNAseq) using the cerebellum of P10 and P17 mice. They showed that the BGs, IGL astrocytes, and WM astrocytes of P10 mice did not significantly differ in gene

expression profiles from the respective astroglial cells of P17 (Mockenhaupt *et al*., 2023). Considering our findings together with those of Mockenhaupt et al., it is plausible that the composition of astroglial cell types in the mouse cerebellum remains stable beyond P10.

In experiments in which hGFAP-eGFP and CAG-mCherry were simultaneously introduced into P0 mice, samples fixed one day after electroporation showed that 1–2 astroglial lineage cells per lobule were labeled with eGFP (Fig. 5b, e). In contrast, samples fixed ten days post-electroporation exhibited labeling of 4–5 astroglial lineage cells per lobule with eGFP (Fig. 6b, c). These results indicate that BGLPs labeled at P0 proliferated, resulting in an increased number of astroglial lineage cells over time. Furthermore, in samples fixed one day after electroporation, the proportion of hGFAP-eGFP-positive cells (representing astroglial lineage cells) among CAG-mCherry-labeled cells (which included GCPs and astroglial lineage cells) was approximately 9% (Fig. 5c, h). This proportion increased to around 41% in samples fixed ten days post-electroporation (Fig. 6b, f). This increase likely reflects a dramatic reduction in the number of GC lineage cells labeled by CAG-mCherry, possibly due to dilution of fluorescence through cell division or selective loss of labeled GC lineage cells via cell death.

To elucidate the molecular differences between BGLPs at P0 and P6, we performed spatial transcriptomics analysis. To our knowledge, this is the first study to successfully isolate the BGLP cluster using spatial transcriptomics. By comparing BGLP sub-clusters from P0 and P6 mice, we found that BGLPs in P0 mouse exhibited more stem cell-like properties, whereas BGLPs in P6 mouse displayed stronger BG-like features. These differences in the molecular properties of BGLPs at P0 and P6 suggest that lineage restriction in BGLPs is primarily driven by intrinsic causes, such as changes in the chromatin state. However, we cannot exclude the possibility of extrinsic causes, such as the increased distance resulting from cerebellar cortex expansion at P6, which may prevent BGLPs from contributing to WM astrocyte production.

In mouse cerebellar scRNA-seq analysis, a cell population referred to as “ciliated cells” is in some cases separated as an independent cluster (Essen et al., 2020). Ciliated cells are known to highly

express genes such as *Dynlrb2*, *Foxj1*, and *Rsph1* which are associated with ciliogenesis and primary ciliary dyskinesia (Essen et al., 2020). Interestingly, although ciliated cells also strongly express astroglial cell markers such as *Sox2*, *Sox9*, and *Fgfr1*, their anatomical localization has not been clearly defined. In our study, we also isolated a cluster of ciliated cells (Fig. 7c). Based on their histological localization, we propose that these cells likely correspond to ependymal cells in the postnatal mouse cerebellum (Supplemental Fig. 3w). This interpretation is further supported by the known characteristics of ependymal cells which possess numerous motile cilia to supply essential nutrients from the cerebrospinal fluid to the brain (Ji et al., 2022).

Through the spatial transcriptomics analysis, we identified BGLP sub-clusters using unsupervised clustering. Sub-cluster annotation was guided by BG-like cell-specific markers (Mecklenburg *et al.*, 2014, Ageta-Ishihara *et al.*, 2013, Saab *et al.*, 2012, Bartsch *et al.*, 1992), proliferative markers, and spatial information. We consider that the integration of spatial information substantially enhances the accuracy of sub-cluster annotation. Interestingly, genes such as *Slc6a11* (previously reported as an astrocyte-like cell marker; Boddum *et al*., 2016), *Cyp26b1* (previously reported as an IGL astrocyte specific marker; Mockenhaupt *et al*., 2023), and *C4b* (previously reported as a WM astrocyte specific marker; Mockenhaupt *et al*., 2023) were not detected as DEGs between each astroglial lineage cell sub-cluster in this study. Whether these genes truly serve as markers for specific astroglial lineage subtypes remains to be determined in future investigations.

Our *in vivo* and *in silico* analyses revealed that BGLPs in neonatal (P0) mice possess greater pluripotency compared to those in P6 mice. It has also been reported that, in neonatal mice, BGLPs can undergo trans-differentiation to compensate for the loss of GCPs following radiation-induced depletion (Bayin et al., 2021). Together, these findings suggest that BGLPs in neonatal mice represent highly pluripotent stem-like cells. However, the biological significance of this high level of pluripotency remains unknown, and further investigation will be required to elucidate its functional implications.

Experimental procedures

Animals

All animal experiments were approved by the Animal Care and Use Committee of the National Institute of Neuroscience, National Center of Neurology and Psychiatry (Tokyo, Japan; Project 202017R2). ICR mice were used in all animal experiments. ICR mice were purchased from SLC. The mice were raised under SPF conditions, with a 12-h light/dark cycle, and were allowed to freely eat and drink food and water. Both male and female mice were used in this study.

Plasmids

The hGFAP-eGFP vector was constructed by removing iCre from the purchased hGFAP promoter-driven eGFP-T2A-iCre vector (VB1131; Vector Biolabs) using restriction enzyme digestion. CAG-mCherry was provided by Dr. N. Masuyama.

In vivo electroporation

In vivo electroporation of postnatal mice has been previously described (Adachi *et al*., 2021). Briefly, expression plasmids were diluted to 1 µg/µL with Milli-Q water. Fast Green was added to achieve a concentration of 0.02% to visualize the plasmid solution. The pups were anesthetized on ice before electroporation, and 10 µL of plasmid solution was injected onto the surface of the cerebellar vermis region of P0 or P6 pups. For P0 and P6, electrical pulses of 70 V and 80 V, respectively, were used for electroporation. The other conditions for the electric pulse were the same for both stages (pulse length of 50 ms, pulse interval of 150 ms, and seven times). Forceps-type electrodes (CUY650P5-3, NEPA) were used for electroporation. After electroporation, the pups were kept warm at 37 °C until they recovered and then returned to their litter. In this experimental method, genes were mainly introduced into lobules IV–VI of the cerebellar vermis. During electroporation of hGFAP-eGFP, CAG-mCherry was co-introduced for normalization purposes.

Immunohistochemistry and antibodies

Mice less than 10 days old were decapitated, and their brains were collected and shaken while immersed in 4% PFA solution overnight. Mice older than 10 days were perfused and fixed, and their brains were collected and shaken while immersed in a 4% PFA solution overnight. The brains soaked in 4% PFA were then soaked in 1×PBS, 10% sucrose, and 30% sucrose overnight and shaken. The brains were then embedded in an O.C.T compound (Sakura Finetek). Frozen brains were sagittally sectioned at a thickness of 16 μm using a cryostat (CM3050 S; Leica). Cryosections were washed twice with PBS for 10 min and then incubated at room temperature with 10% normal donkey serum (S30-100ML; Millipore) containing 0.2% PBST (Triton) for 40 min. After blocking, the sections were incubated with primary antibodies diluted with blocking solutions at 4 °C for 16 h. The following primary antibodies were used: mouse anti-CalbinidinD28K (1:500; C9848; Sigma-Aldrich), rat anti-GFAP (1:500; AB5541; Merck Millipore), chicken anti-GFP (1:1000; ab1218; Abcam), rat anti-Ki67 (1:500; 14-5698-82; Invitrogen), goat anti-NeuroD1 (1:500; AF2746; R&D), goat anti-Olig2 (1:500; AF2418; R&D Systems), rabbit PAX2 (1:500; 71-6000; Invitrogen), rabbit anti-PAX6 (1:500, 901301; Biolegend), rabbit anti-RFP (1:500; PM005; MBL), rat anti-RFP (1:1000; 5F8-20; Proteintech Group, Inc.), goat anti-Human SOX9 (1:500; AF3075; R&D Systems), rabbit anti-Tbr2/Eomes (1:1000; ab183991; Abcam), and rabbit anti-Vimentin (1:500; D21H3; Cell Signaling). Subsequently, slides were rinsed with PBS (10 min, twice) and incubated with secondary antibodies conjugated with Alexa Fluor 405, Alexa Fluor 488, Alexa Fluor 568, Alexa Fluor 647 (1:400; Abcam), or Alexa Fluor 488 (1:400; Jackson) and DAPI (25 μg/mL; Invitrogen) in 0.2% PBST at room temperature for 2 h. The slides were rinsed again with PBS (10 min, twice) and mounted with ProLong Glass Antifade Mountant (P36984; LTJ).

Image acquisition and quantification

The entire sagittal section of the cerebellar vermis was observed under a microscope and analyzed to examine the distribution of astroglial cells in mice at each stage of the experiment. In the experiment

that introduced genes by electroporation, lobules IV to VI of the cerebellar vermis were observed under a microscope and analyzed. At least two images were obtained from each participant. Images were obtained using a confocal microscope, SpinSR10 (Olympus). The acquired images were adjusted and analyzed using ImageJ software (RSB). All graphs were generated using GraphPad Prism software (GraphPad Software).

Xenium experiment

FFPE brain samples from ICR P0 and P6 mice were sectioned into 5 μm slices and placed onto Xenium slides. The Xenium Prime 5 K Mouse Pan Tissue and Pathways Panel, which targets 5001 genes, was used for the experiment. Deparaffinization, decrosslinking, probe hybridization, ligation, and signal detection were performed according to the manufacturer's protocol. Cell segmentation and transcript counting were automatically performed using the Xenium Analyzer.

Xenium data processing

Regions of interest (ROIs) covering the entire cerebellum of P0 and P6 mice were manually selected using Xenium Explorer (version). The ROIs contained 5,146 cells from P0 mouse and 19,892 cells from P6 mouse. Cell ID information is provided in the supplementary file.
Data analysis was conducted in R (v4.4.2) using the Seurat package (v5.2.1). Gene expression data from the P0 and P6 cerebellum were merged and filtered using the criteria (nCount > 300 and nFeature > 300). After quality filtering, log normalization, dimensionality reduction, and clustering were performed using Seurat functions with default parameters. This analysis resulted in the identification of 24 clusters. Each cluster was annotated based on marker gene expression(reference) and spatial information. Clusters 6, 11, and 13, identified as astroglial lineage clusters, were extracted for subclustering. To remove the influence of cell cycle-related gene expression, cell cycle scoring and regression were performed (citation), followed by dimensionality reduction and clustering, which yielded 10 sub-clusters. Among these, sub-

clusters 7 (BGLPs at P0) and 1 and 4 (BGLPs at P6) were identified as BGLP clusters based on marker gene expression, cell morphology, and spatial localization. Differential expression analysis between BGLP clusters from the P0 and P6 cerebellum was performed using Seurat's FindMarkers function. Differentially expressed genes (DEGs) were defined by an adjusted p-value < 0.05 and $\log_2$ fold change. Gene Ontology (GO) enrichment analysis was performed on the DEGs using the clusterProfiler package (v4.14.4), focusing on the top 20 categories of the "Biological Process" ontology. A heatmap was generated using DEGs with an average $\log_2$ fold change > 1 and adjusted p-value < 0.05. To identify potential upstream transcription factors potentially regulating the expressions of DEGs, enrichment analysis was conducted using the enrichR package (Chen et al., 2013) separately for the 224 and 88 DEGs. Among the enriched transcription factors, *Foxm1* was identified for P0 BGLP DEGs and *Nfia* for P6 BGLP DEGs. All codes for generating results are available in the Hoshino Lab GitHub repository.

Statistical analyses

Individual animals or trials were considered as biological replicates. All mice were prepared under identical experimental conditions. All data are presented as mean ± SEM. All statistical analyses were performed using GraphPad Prism software (GraphPad Software). Statistical tests were performed using Sidak's multiple comparison tests; p values are represented as N.S. for $p > 0.05$; $*p < 0.05$, $**p < 0.01$, and $***p < 0.001$.

Acknowledgements

This work was supported by JSPS KAKENHI (Grant Numbers JP22H02730 to MH, 21K20853 and 23K14203 to TA); AMED (Grant Numbers 24wm0425005h0004 and 24ek0109764h0001 to MH), an Intramural Research Grant of NCNP (4–5, 4-6, 6-9 to MH); Japan Health Research Promotion Bureau (JH) under Research Fund (2020-B-07 and 2024-D-01 to MH); Multilayered Stress Diseases (JPMXP1323015483 to MH), Tokumori Yasumoto Memorial Trust (MH) and Takeda Science Foundation (Grants 2024049458 to TA). We would like to thank Editage (www.editage.jp) for English

language editing.

Author contributions

T.A. and M.H. supervised this project. K.S., T.A., T.O. and M.H. designed the study. K.S., T.A. and M.H. wrote the manuscript. K.S., T.A., E.I., I.H., M.M. and J.K. performed *in vivo* experiments and statistical analysis. K.N. and S.M. performed spatial transcriptomics analysis preparation. K.S., S.M. and T.O. performed spatial transcriptomics analysis.

References

1. Vivi, E. & Di Benedetto, B. Brain stars take the lead during critical periods of early postnatal brain development: relevance of astrocytes in health and mental disorders. *Mol. Psychiatry* 29, 2821–2833 (2024).
2. Khakh, B. S. & Sofroniew, M. V. Diversity of astrocyte functions and phenotypes in neural circuits. *Nat. Neurosci*. 18, 942–952 (2015).
3. Leto, K. *et al.* Consensus Paper: Cerebellar Development. *Cerebellum* **15**, 789–828 (2016).
4. Joyner, A. L. & Bayin, N. S. Cerebellum lineage allocation, morphogenesis and repair: impact of interplay amongst cells. *Development* **149**, dev185587 (2022).
5. Cerrato, V. *et al.* Multiple origins and modularity in the spatiotemporal emergence of cerebellar astrocyte heterogeneity. *PLOS Biology* **16**, e2005513 (2018).
6. Bayin, N. S. *et al.* Injury-induced ASCL1 expression orchestrates a transitory cell state required for repair of the neonatal cerebellum. *Science Advances* **7**, eabj1598 (2021).
7. Adachi, T. *et al.* Notch Signaling between Cerebellar Granule Cell Progenitors. *eNeuro* **8**, (2021).
8. Miyashita, S. *et al.* Cyclin D1 controls development of cerebellar granule cell progenitors through phosphorylation and stabilization of ATOH1. *The EMBO Journal* **40**, e105712 (2021).
9. Yamashita, M. *et al.* The role of SCFSkp2 and SCFβ-TrCP1/2 in the cerebellar granule cell precursors. *Genes to Cells* **25**, 796–810 (2020).
10. Owa, T. *et al.* Meis1 Coordinates Cerebellar Granule Cell Development by Regulating Pax6 Transcription, BMP Signaling and Atoh1 Degradation. *J. Neurosci.* **38**, 1277–1294 (2018).
11. Vladoiu, M. C. *et al.* Childhood cerebellar tumours mirror conserved fetal transcriptional programs. *Nature* **572**, 67–73 (2019).
12. Machold, R. & Fishell, G. Math1 Is Expressed in Temporally Discrete Pools of Cerebellar Rhombic-Lip Neural Progenitors. *Neuron* **48**, 17–24 (2005).
13. Chen, E. Y. *et al*. Enrichr: interactive and collaborative HTML5 gene list enrichment analysis tool. *BMC Bioinformatics* 14, 128 (2013).
14. Mockenhaupt, K. *et al.* Yin Yang 1 controls cerebellar astrocyte maturation. *Glia* **71**, 2437–2455 (2023).

12. Mecklenburg, N. *et al*. Growth and differentiation factor 10 (Gdf10) is involved in Bergmann glial cell development under Shh regulation. *Glia* 62, 1713–1723 (2014).

13. Ageta-Ishihara, N. *et al*. Chronic overload of SEPT4, a parkin substrate that aggregates in Parkinson's disease, causes behavioral alterations but not neurodegeneration in mice. *Mol. Brain* 6, 35 (2013).
14. Saab, A. S. *et al*. Bergmann Glial AMPA Receptors Are Required for Fine Motor Coordination. *Science* 337, 749–753 (2012).
15. Bartsch, S. *et al*. Expression of tenascin in the developing and adult cerebellar cortex. J. *Neurosci*. 12, 736–749 (1992).
16. Boddum, K. *et al.* Astrocytic GABA transporter activity modulates excitatory neurotransmission. *Nat. Commun*. 7, 13572 (2016).
17. Essen, M. J. V *et al*. Deconstructing cerebellar development cell by cell. *PLOS Genetics*. 16(4) (2020)
18. Ji, W. *et al*. Ependymal Cilia: Physiology and Role in Hydrocephalus. Front. *Mol. Neurosci*. Volume 15 (2022)

Figure legends

Fig1. Distribution of astroglial lineage cells in the postnatal mouse cerebellum

(a) Immunostaining of the P0 and P10 mice cerebellum with DAPI, SOX9, KI67, VIMENTIN and GFAP; Scale bars: 200 µm (left panels), 20 µm (right panel). (b) Number of each astroglial progenitors in P0, P2, P4, P6, P8, P10 and P21 mouse cerebellar sections. Bergmann glia-like progenitor (BG-like progenitor) is SOX9 and KI67 double positive and has unipolar fibers (stained with VIMENTIN or GFAP). Astrocyte-like progenitor is SOX9 and KI67 double positive and has multipolar fibers (stained with VIMENTIN or GFAP). (c) Number of each astroglial cells in P0, P2, P4, P6, P8, P10 and P21 mouse cerebellar sections. Bergmann glial cell (BG) is SOX9 positive and KI67 negative, and has unipolar fibers (stained with VIMENTIN or GFAP). Astrocyte is SOX9 positive and KI67 negative and has multipolar fibers (stained with VIMENTIN or GFAP).

Fig2. Electroporation to P0 and P6 mouse cerebellar surface with CAG-mCherry labels only GC lineage cells and BG-like cells

(a-d) Immunostaining with DAPI, RFP (for enhancing mCherry), CalbindinD28K, PAX6, TBR2, OLIG2, PAX2, SOX9 and VIMENTIN in the P1 mouse cerebellum; Scale bars: 50µm for (b), (c) and lower magnification panel of (a) and (d). 30 µm, 10 µm for higher magnification panel of (a) and (d),

respectively. The white arrowheads in (a) indicate GC lineage cells that are positive for both PAX6 and mCherry which are localized to EGL. The white arrowhead in (d) indicates Bergmann glia-like cell (BG-like cell) that is positive for both SOX9 and mCherry and has unipolar projections. (e) mCherry+ cell number per electroporated lobule. Animal numbers: *N=5* for the analysis. (f) Unipolar Brush Cell (UBC) is TBR2 positive cell; *N=4*. Oligodendrocyte lineage (OL lineage) is OLIG2 positive cell; *N=4*. Interneuron (IN) is PAX2 positive cell; *N=3*. Purkinje Cell (PC) is CalbindinD28K positive cell; *N=5*. Granule Cell lineage (GC lineage) is PAX6 positive EGL localizing cell; *N=5*. BG-like cell is SOX9 positive and has unipolar fibers (stained with VIMENTIN); *N=4*. Astrocyte-like cell is SOX9 positive and has multipolar fibers (stained with VIMENTIN); *N=4*. (g) Immunostaining with DAPI, RFP (mCherry), SOX9, KI67 in P1; Scale bars: 40 µm. White arrowhead indicates BGLP that is positive for SOX9, KI67, and mCherry and has unipolar projections. White open arrowhead indicates BG that is positive for SOX9 and mCherry and has unipolar projections and is negative for KI67. (h) KI67+ cell rate in SOX9+ mCherry+ cells; *N=7*. (i-l) Immunostaining with DAPI, RFP (mCherry), CalbindinD28K, PAX6, TBR2, OLIG2, PAX2, SOX9 and GFAP in P7 mice cerebellum; Scale bars: 50µm for (j), (k) and lower magnification panel of (i) and (l). 30 µm, 10 µm for higher magnification panel of (i) and (l), respectively. The white arrowheads in (i) indicate GC lineage cells that are positive for both PAX6 and mCherry which are localized to EGL. The white arrowhead in (l) indicates BG-like cell that is positive for both SOX9 and mCherry and has unipolar projections. (m) mCherry+ cell number per electroporated lobule; *N= 6* for the analysis. (n) The markers for UBC, OL lineage, IN, PC and GC lineage used the same antibodies as P1. Animal numbers: *N=4* for UBC, OL lineage, *N=5* for IN, and *N=6* for PC and GC lineage. BG-like cell is SOX9 positive and has unipolar fibers (stained with GFAP); *N=4* for the analysis. Astrocyte-like cell is SOX9 positive and has multipolar fibers (stained with GFAP); *N=4* for the analysis. (o) Immunostaining with DAPI, RFP (mCherry), SOX9, KI67 in P7; Scale bars: 40 µm. White arrowhead indicates BGLP that is positive for SOX9, KI67 and mCherry, and has unipolar projections. White open arrowhead indicates BG that is positive for SOX9 and mCherry and has unipolar projections and is negative for KI67. (p) KI67+

cell rate in SOX9+ mCherry+ cells; *N=4* for the analysis. All data are shown as mean ± SEM.

Fig3. P0 mouse BGLPs labeled with CAG-mCherry differentiate into BGs, IGL-localized astrocytes and WM-localized astrocytes in P10 mouse cerebellum

(a) Experimental scheme. CAG-mCherry vector was introduced into P0 or P6 mouse cerebellar surface by electroporation. Electroporated mouse were fixed at P10. (b) Immunostaining with SOX9, GFAP, RFP (mCherry) in P10; Scale bars: 100 µm (left panels) and 50 µm (right panels). (c) mCherry+ SOX9+ cell number per electroporated lobule; *N=6* for both stage analysis. (d) mCherry+ SOX9+ cell rate in mCherry+ cells; *N=6* for both stage analysis. (e) Distribution of mCherry+ astroglial cells; *N=6* for both stage analysis. Statistical tests were performed by Sidak's multiple comparisons test; *p* values were represented as; N.S. for $p > 0.05$; $*p < 0.05$, $***p < 0.001$. All data are shown as mean ± SEM.

Fig4. P0 mouse BGLPs labeled with CAG-mCherry differentiate into BGs, IGL astrocytes and WM astrocytes in P30 mouse cerebellum

(a) Experimental scheme. CAG-mCherry vector was introduced into P0 or P6 mouse cerebellar surface by electroporation. Electroporated mouse were fixed at P30. (b)Immunostaining with SOX9, GFAP, RFP (mCherry) at P30; Scale bars: 100 µm (left panels) and 70 µm (right panels). (c) mCherry+ SOX9+ cell number per electroporated lobule; *N=6* for P0EP-P10 Fix, P0EP-P30Fix, P6EP-P10Fix and *N=9* for P6EP-P30Fix; N.S > 0.05, Sidak's multiple comparisons test. (d) mCherry+ SOX9+ cell rate in mCherry+ cells; *N=6* for P0EP-P10 Fix, P0EP-P30Fix, P6EP-P10Fix and *N=9* for P6EP-P30Fix; N.S > 0.05, Sidak's multiple comparisons test. (e, f) Distribution of mCherry+ astroglial cells; *N=6* for P0EP-P10 Fix, P0EP-P30Fix, P6EP-P10Fix and *N=9* for P6EP-P30Fix; N.S > 0.05, $***p < 0.001$, Sidak's multiple comparisons test. All data are shown as mean ± SEM.

Fig5. Electroporation to P0 mouse cerebellar surface with hGFAP-promoter labels BGLPs specifically and sparsely

(a) Experimental scheme. hGFAP-eGFP vector and CAG-mCherry vectors were introduced into mouse cerebellum at P0 and fixed at P1. (b) Immunostaining with SOX9, VIMENTIN, GFP at P1; Scale bars: 100 µm (upper panels) and 50 µm (lower panels). (c) Immunostaining with DAPI, GFP, RFP (mCherry), KI67 at P1; Scale bars: 100 µm (upper panels) and 50 µm (lower panels). (d) Immunostaining with DAPI, GFP, RFP (mCherry), NEUROD1 at P1; Scale bars: 50 µm. (e) GFP+ cell number per electroporated lobule; *N=8* for the analysis. (f) BG-like shape cell rate in GFP+ cells; *N=8* for the analysis. (g) KI67+ cell rate in GFP+ BG-like shape cells; *N=8* for the analysis. (h) GFP+ cell rate in mCherry+ cells; *N=8* for the analysis. All Data are shown as mean ± SEM.

Fig6. P0 mouse BGLPs labeled with hGFAP-eGFP differentiate into BGs, IGL-localized astrocytes and WM-localized astrocytes in P10 mouse cerebellum

(a) Experimental scheme. hGFAP-eGFP and CAG-mCherry vectors were introduced into mouse cerebellum at P0 fixed at P10. (b) Immunostaining with SOX9, GFP, RFP (mCherry), GFAP at P10; Scale bars: 100 µm (left panels) and 40 µm (right panels). (c) GFP+ SOX9+ cell number per electroporated lobule; *N=6* for the analysis. (d) GFP+ SOX9+ cell rate in GFP+ cells; *N=6* for the analysis. (e) Distribution of GFP+ astroglial cells; *N=6* for the analysis. (f) GFP+ cell rate in mCherry+ cells; *N=6* for the analysis. All data are shown as mean ± SEM.

Fig7. Spatial transcriptomics analysis identifies BGLP clusters in P0 and P6 mouse cerebellum

‘(a) Cerebellar slices used for spatial transcriptomics analysis. The panels show region of interests (ROI) which was stained with DAPI. Scale bars: 200 µm for P0 and 500 µm for P6. (b) Uniform manifold approximation and projection (UMAP) dimensional reduction was performed using segmented cells and 24 distinct clusters were identified. (c) Gene expression profiles of each cerebellar cell markers across the 24 identified clusters. Cluster annotation was performed based on the expression profiles of cell markers and spatial localization information. (d) UMAP dimensional reduction was performed using P0 and P6 astroglial lineage cell clusters (Cluster 6, 11, 13). 10 distinct

sub-clusters were identified. (e)-(g) Annotation of each astroglial lineage cell sub-cluster. Annotation was performed based on the expression profiles of BG-like cell specific markers and proliferative marker (e), and spatial localization information (f, g). Scale bars: 200 µm for (f) and 500 µm for (g).

Fig8. P0 mouse BGLPs show higher stem cell marker expression, while P6 mouse BGLPs exhibit elevated BG-like cell specific gene levels

(a) Expression profiles of 311 DEGs between BGLP from P0 and P6 mouse were visualized by heatmap. 224 genes were upregulated in BGLPs at P0, while 87 genes were upregulated in BGLPs at P6. Due to the difference in sex between the P0 and P6 mouse, the identified differentially expressed genes (DEGs) included sex-linked genes, such as *Xist*. (b) GO analysis was performed for the 224 upregulated genes in BGLPs at P0. (c) Box plots of *Nes*, *Sox4* and *Sox11*, genes associated with the maintenance of pluripotency, ***$p < 0.001$. (d) GO analysis was performed for the 87 upregulated genes in BGLPs at P6. (e) Box plots of BG-like cell specific markers, *Gdf10*, *Gria1*, *Tnc* and *Sept4*. ***$p < 0.001$. (f) Box plots of *Foxm1* and *Nfia*, putative upstream regulators of DEGs in BGLPs at P0 and BGLPs at P6, ***$p < 0.001$. (g) A schematic model illustrating the differences in differentiation potential and gene expression profiles of BGLPs between P0 and P6 mice. At P0, BGLPs give rise not only to BGs and IGL astrocytes, but also to WM astrocytes. Compared to BGLPs in P6 mouse, BGLPs in P0 mouse exhibit higher expression of genes associated with stemness. In contrast, BGLPs in P6 mouse show elevated expression of BG-like cell–specific genes.

SupFig1. Results of electroporation to P6 mouse cerebellar surface with hGFAP-promoter

(a) Experimental scheme. The hGFAP-eGFP and CAG-mCherry vectors were introduced into the mouse cerebellum at P6 and fixed at P7. (b) Immunostaining with DAPI, GFP, RFP (mCherry), GFAP in P7; Scale bars: 70 µm. (c) GFP+ cell number per electroporated lobule; $N=4$ for the analysis. (d) BG-like cells in GFP+ cells; $N=4$ for analysis. (e) GFP+ cell rate in mCherry+ cells; $N=4$ for the analysis. All data are shown as mean ± SEM.

SupFig2. Supplemental data for Figure 7

(a) The 24 identified clusters visualized separately for each stage. (b) The 10 identified sub-clusters visualized separately for each stage. (c) Spatial localization information of sub-cluster 8 and 9. (d) Violin plot for annotation only with P0 astroglial lineage sub-clusters. (e)-(h) Feature plot of BG-like cell specific markers (e, f) and proliferative markers (g, h) with P0 astroglial lineage cell sub-clusters. (i) Violin plot for annotation only with P6 astroglial lineage sub-clusters. (j)-(m) Feature plot of BG-like cell specific markers (j, k) and proliferative markers (l, m) with P6 astroglial lineage cell sub-clusters.

SupFig3. Spatial information of each 24 cluster

(a)-(x) Spatial localization information of each 24 cluster at each two stage which was used for annotation. Scale bars: 200 µm (left panels, P0) and 500 µm (right panels, P6).

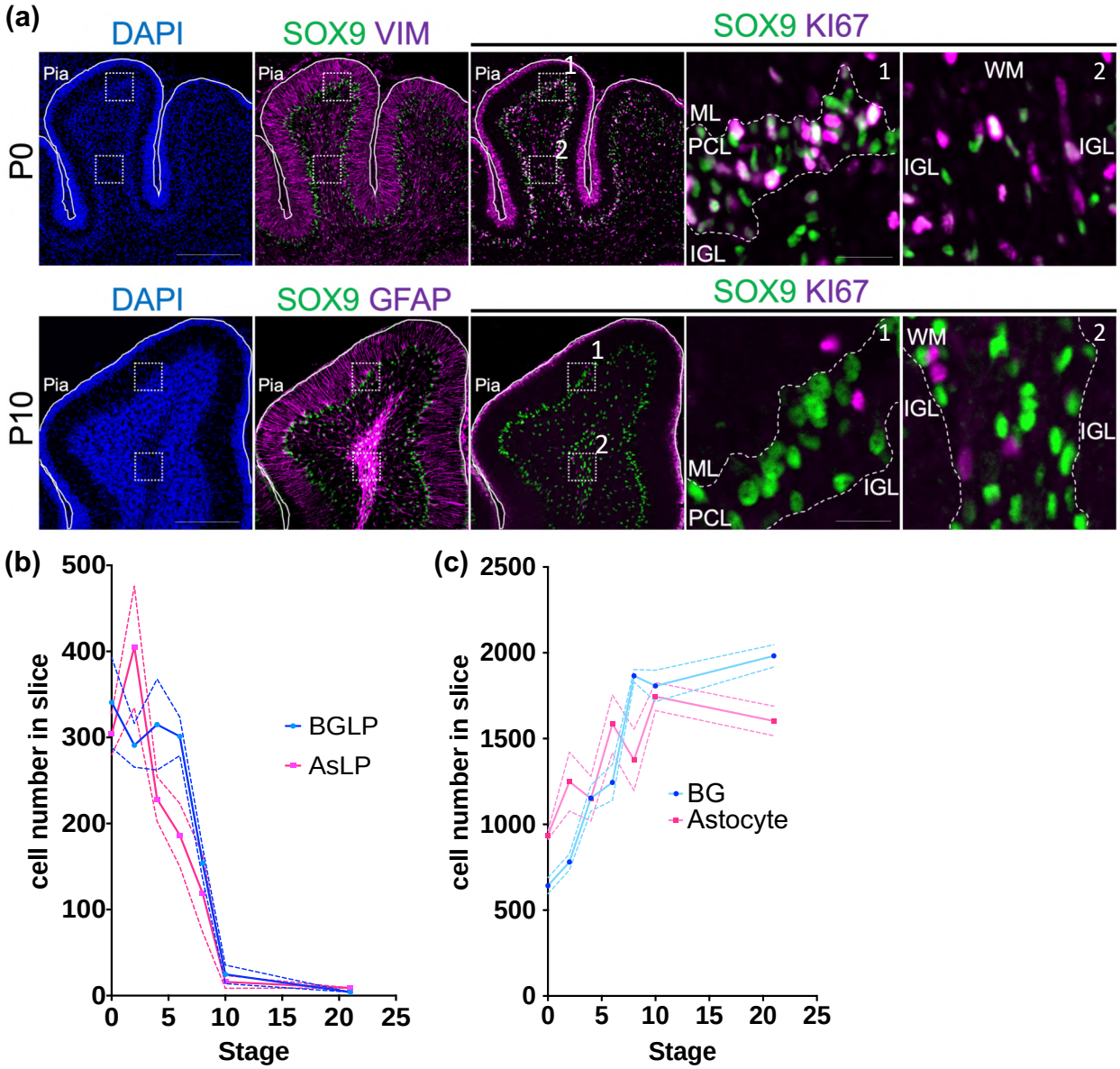

Fig1. Distribution of astroglial lineage cells in the postnatal mouse cerebellum

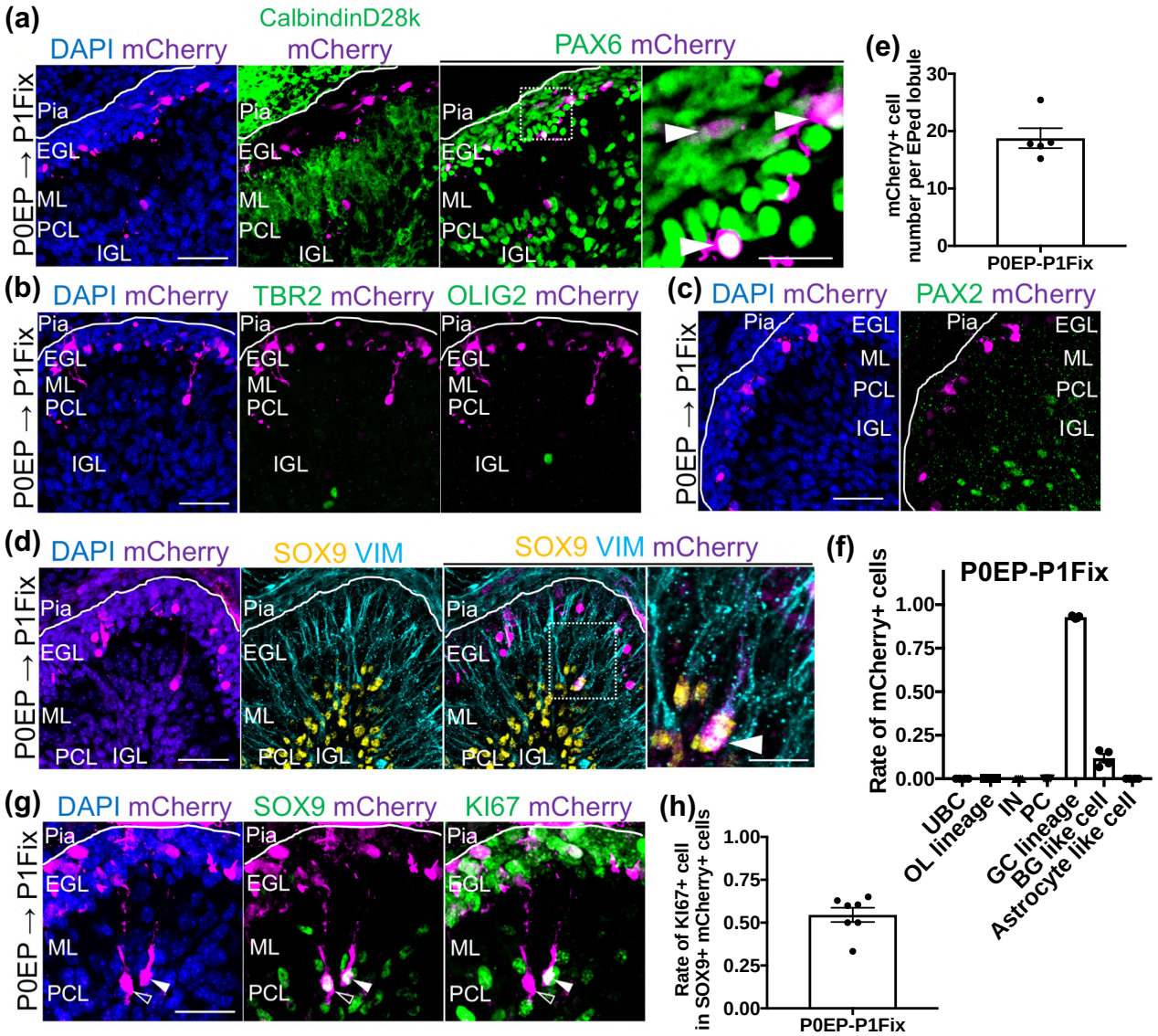

Fig2. Electroporation to P0 and P6 mouse cerebellar surface with CAG-mCherry labels only GC lineage cells and BG-like cells

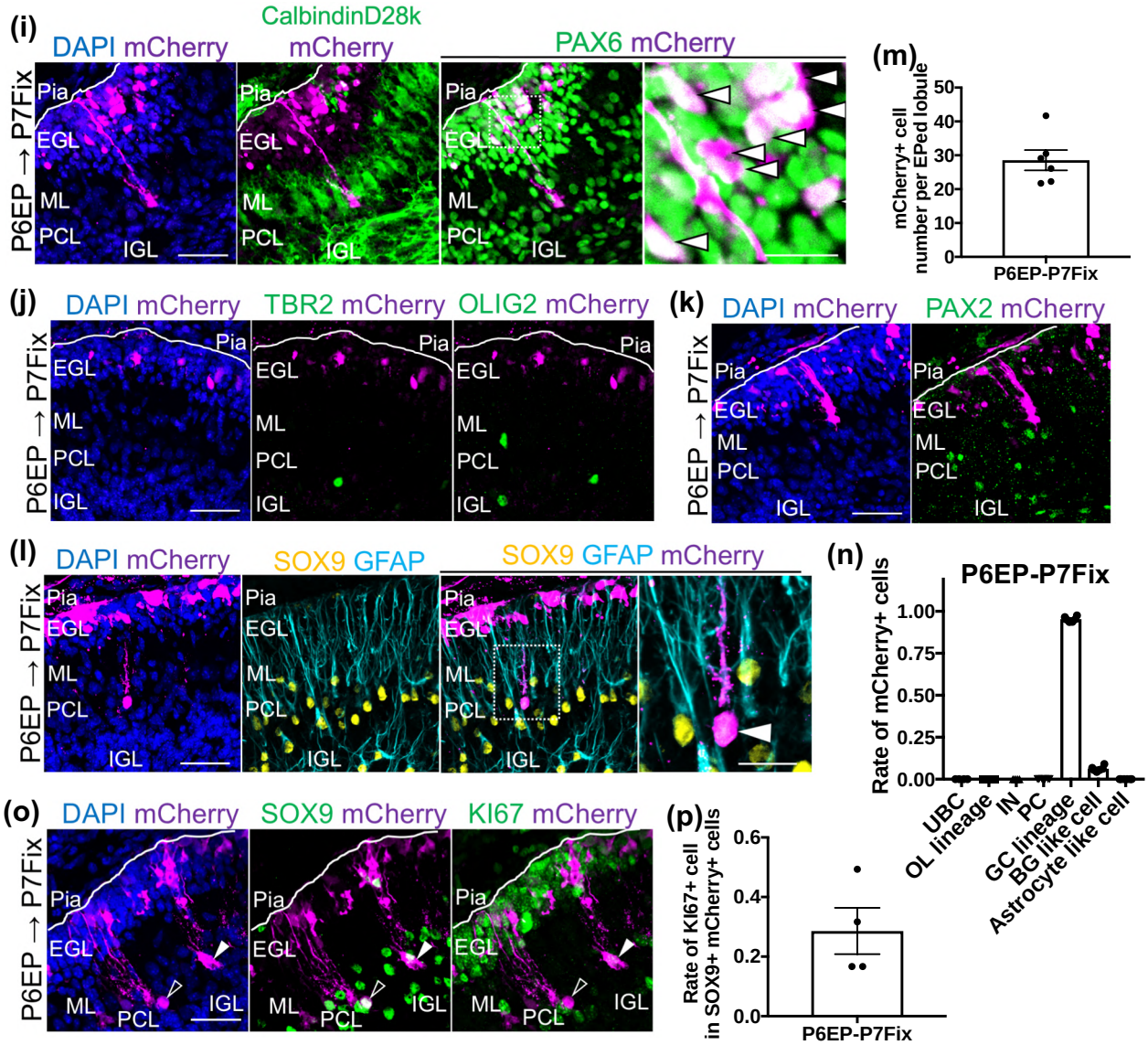

(Continue) Fig2. Electroporation to P0 and P6 mouse cerebellar surface with CAG-mCherry labels only GC lineage cells and BG-like cells

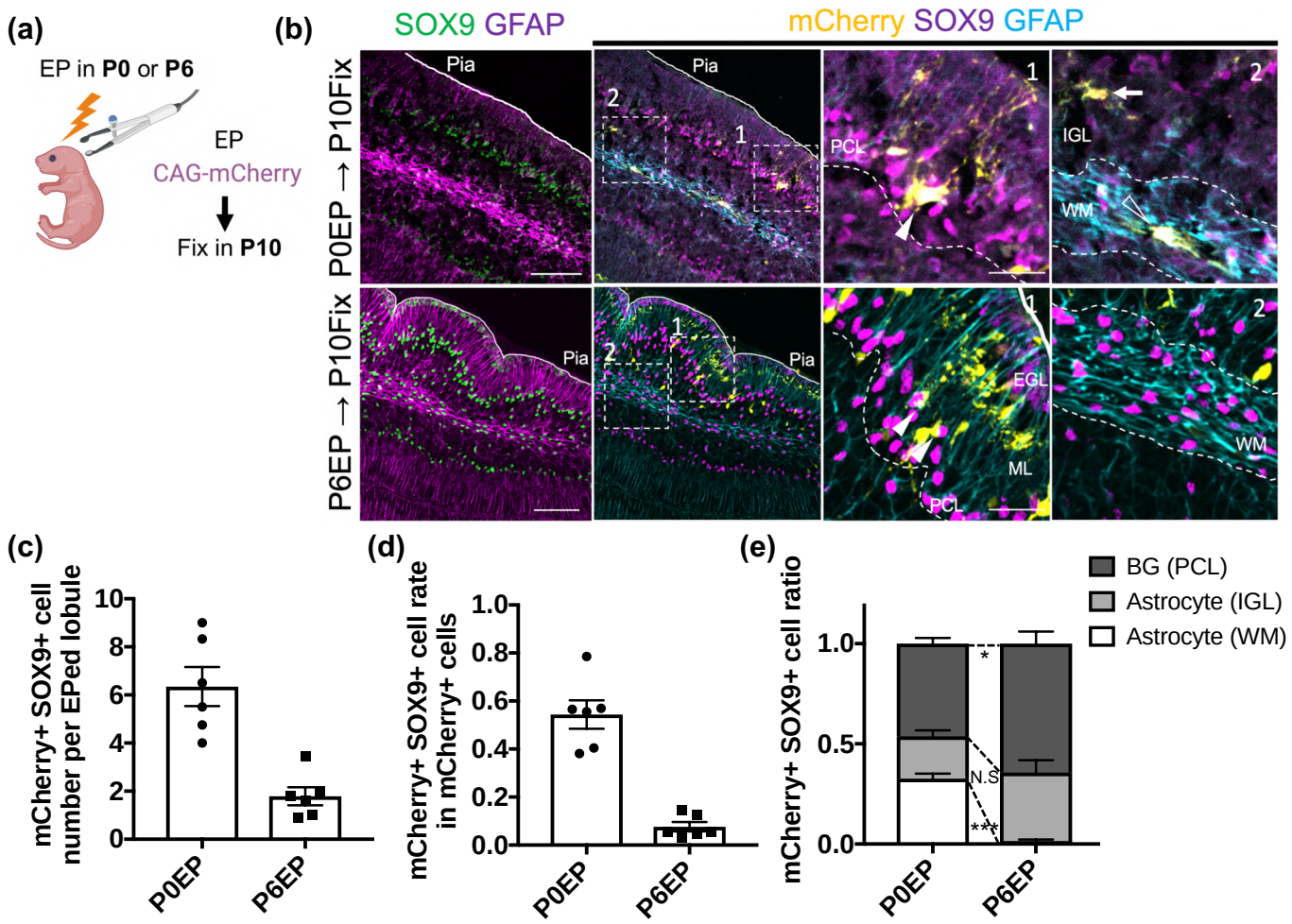

Fig3. P0 mouse BGLPs labeled with CAG-mCherry differentiate into BGs, IGL-localized astrocytes and WM-localized astrocytes in P10 mouse cerebellum

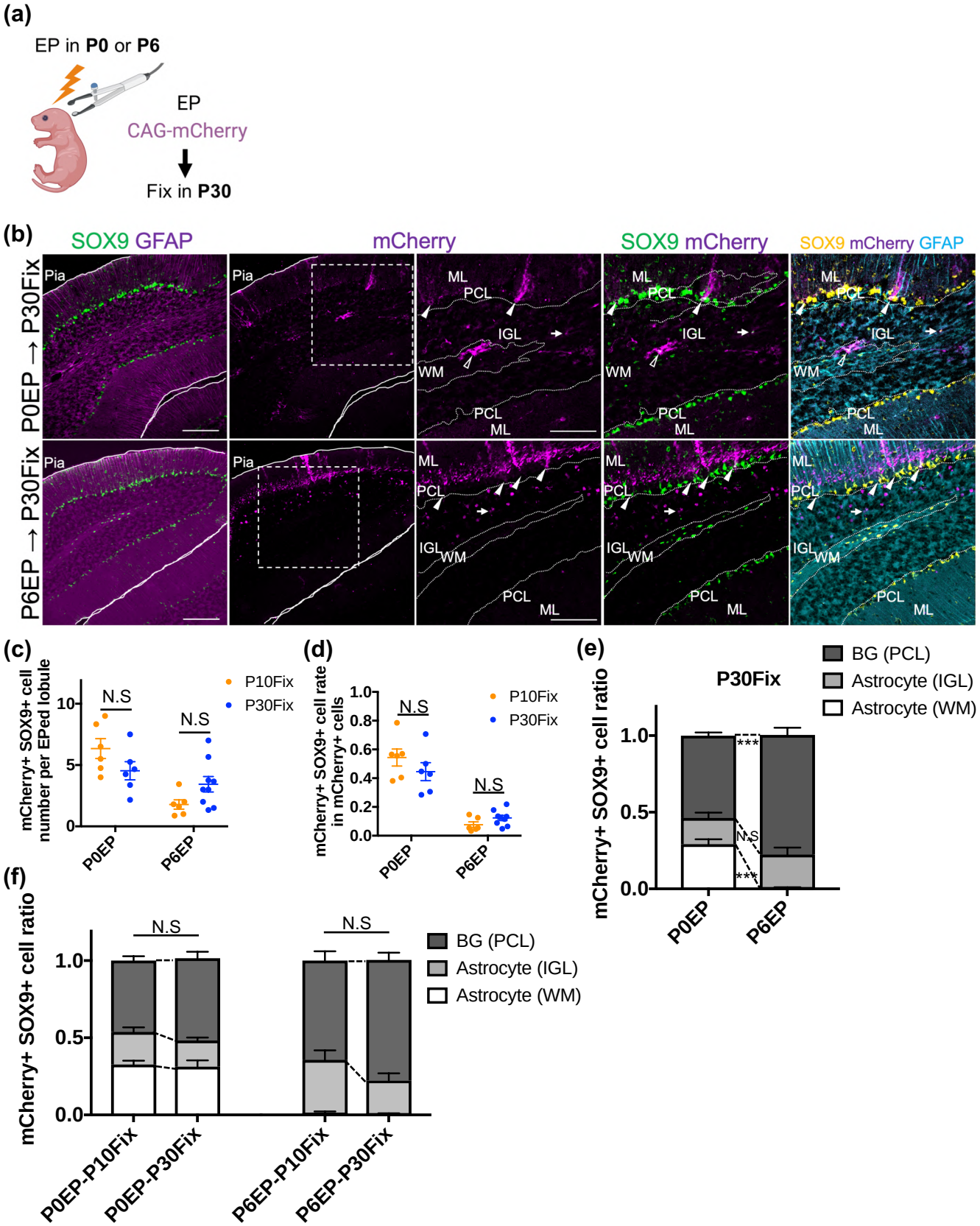

Fig4. P0 mouse BGLPs labeled with CAG-mCherry differentiate into BGs, IGL astrocytes and WM astrocytes in P30 mouse cerebellum

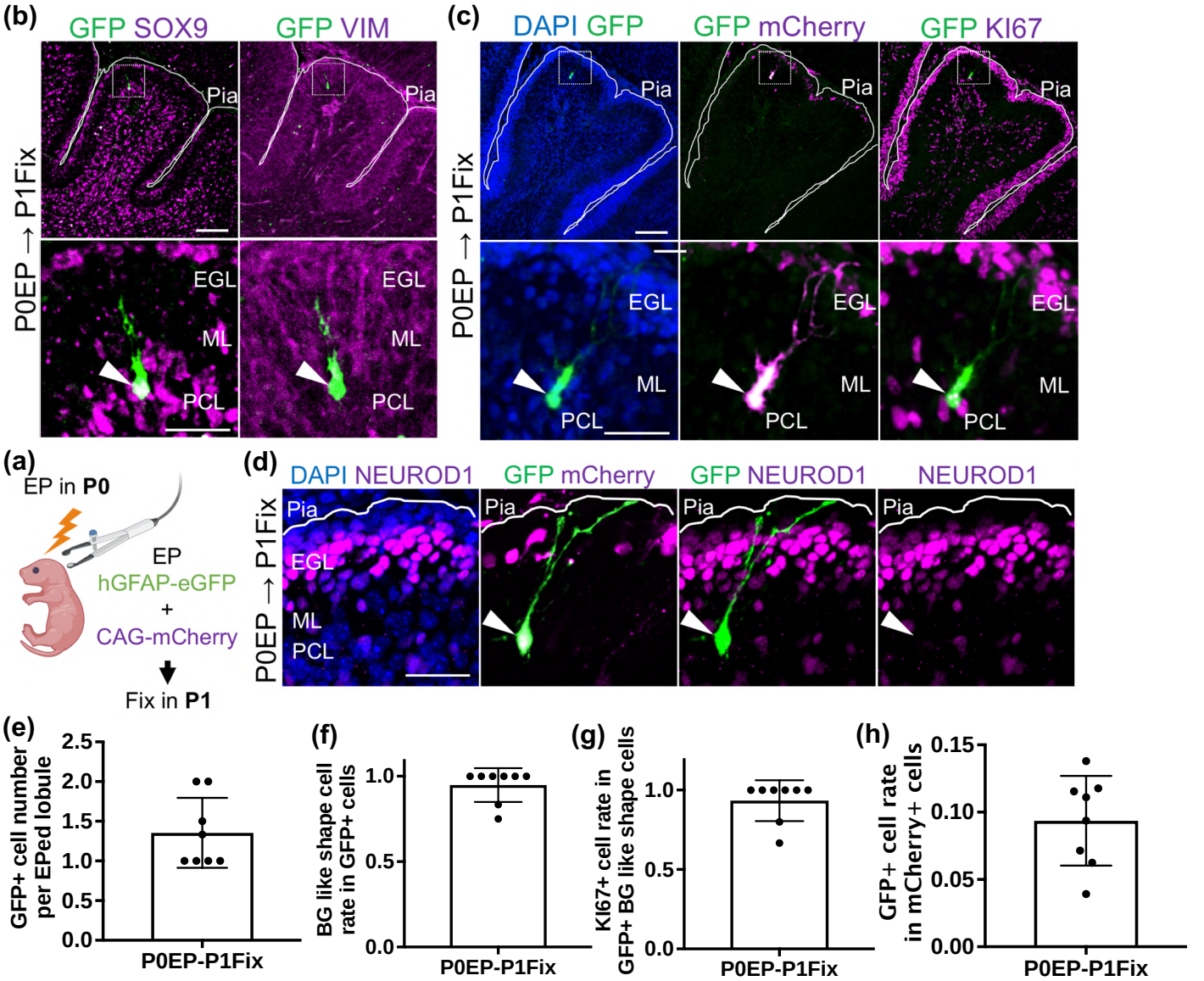

Fig5. Electroporation to P0 mouse cerebellar surface with hGFAP-promoter labels BGLPs specifically and sparsely

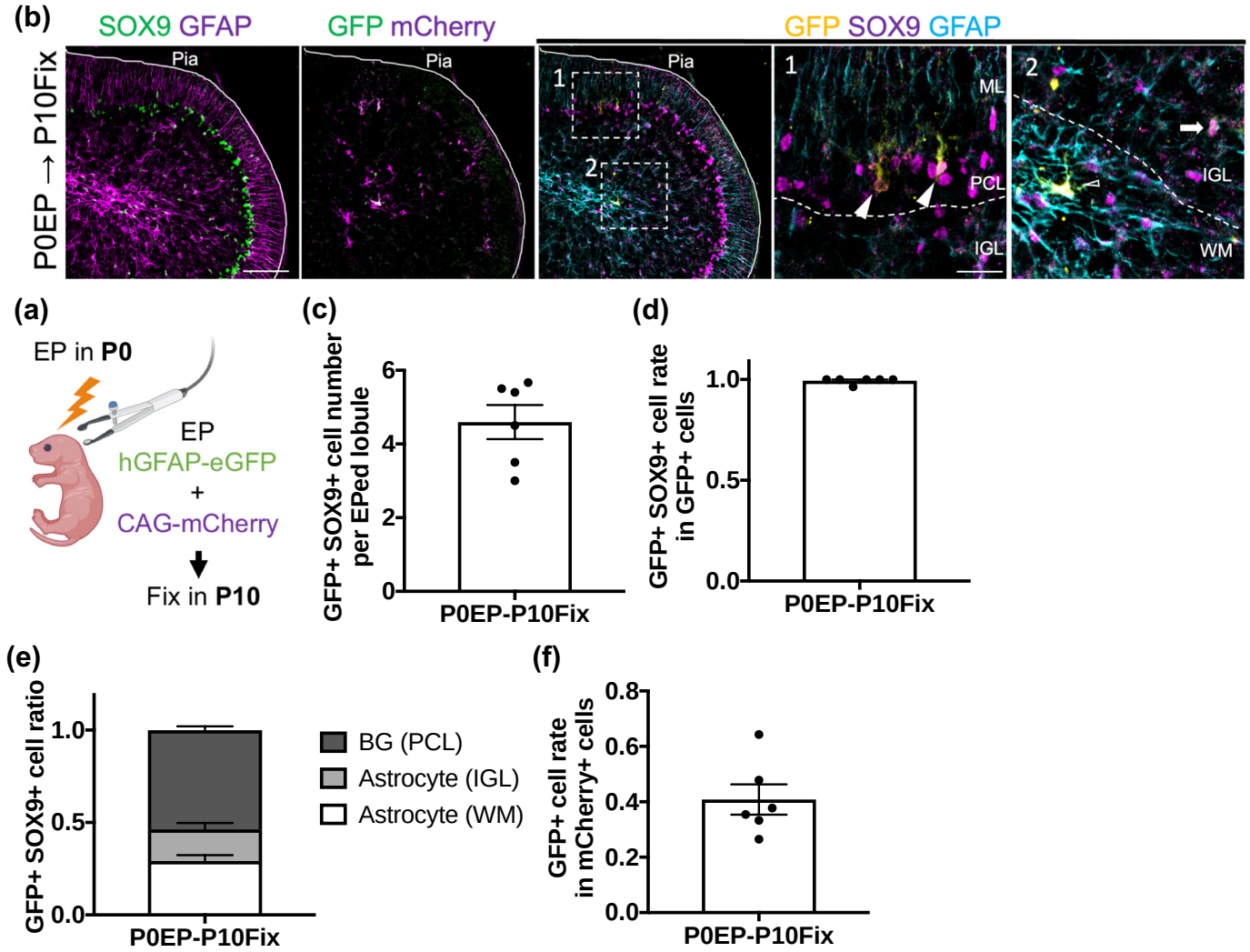

Fig6. P0 mouse BGLPs labeled with hGFAP-eGFP differentiate into BGs, IGL-localized astrocytes and WM-localized astrocytes in P10 mouse cerebellum

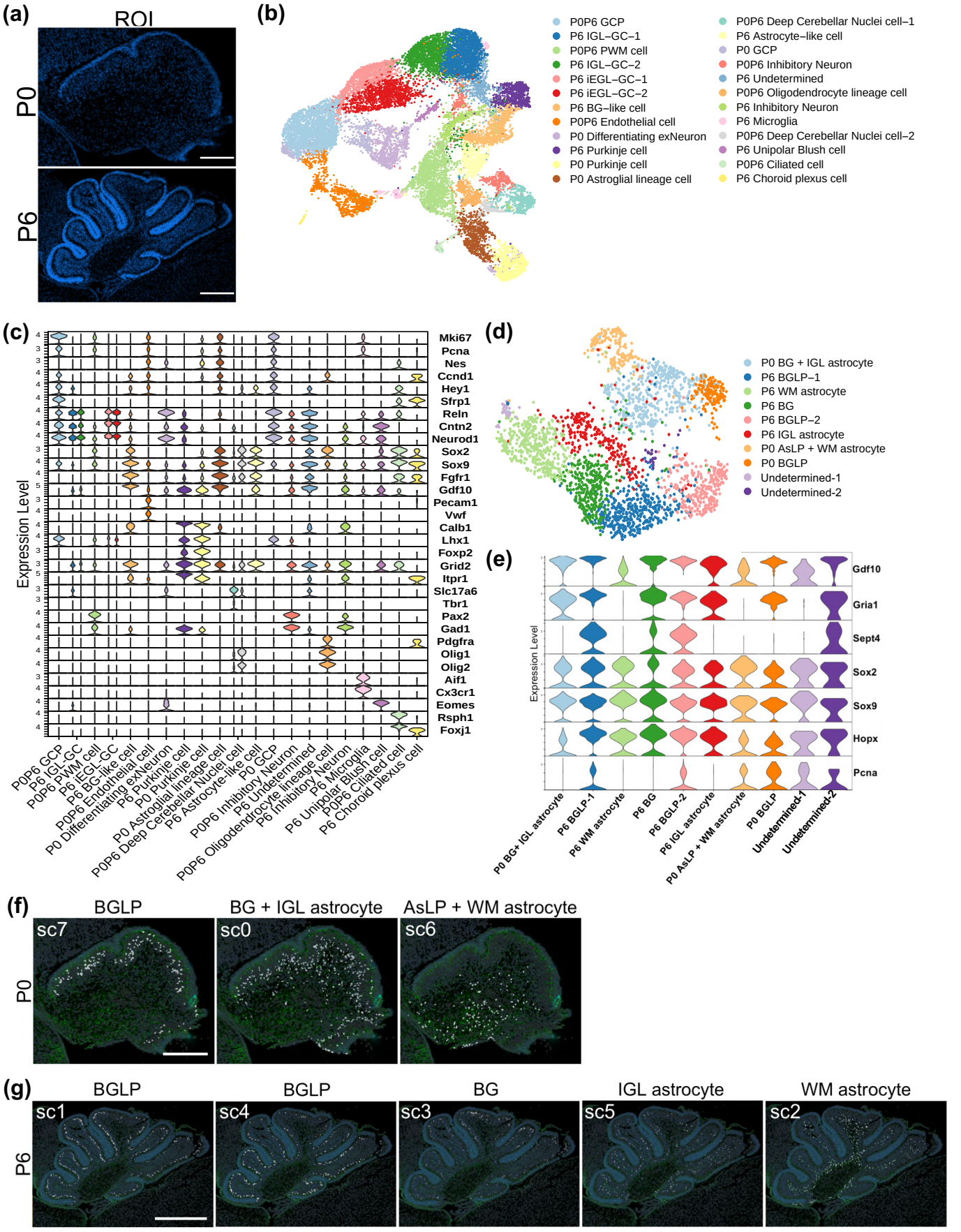

Fig7. Spatial transcriptomics analysis identifies BGLP clusters in P0 and P6 mouse cerebellum

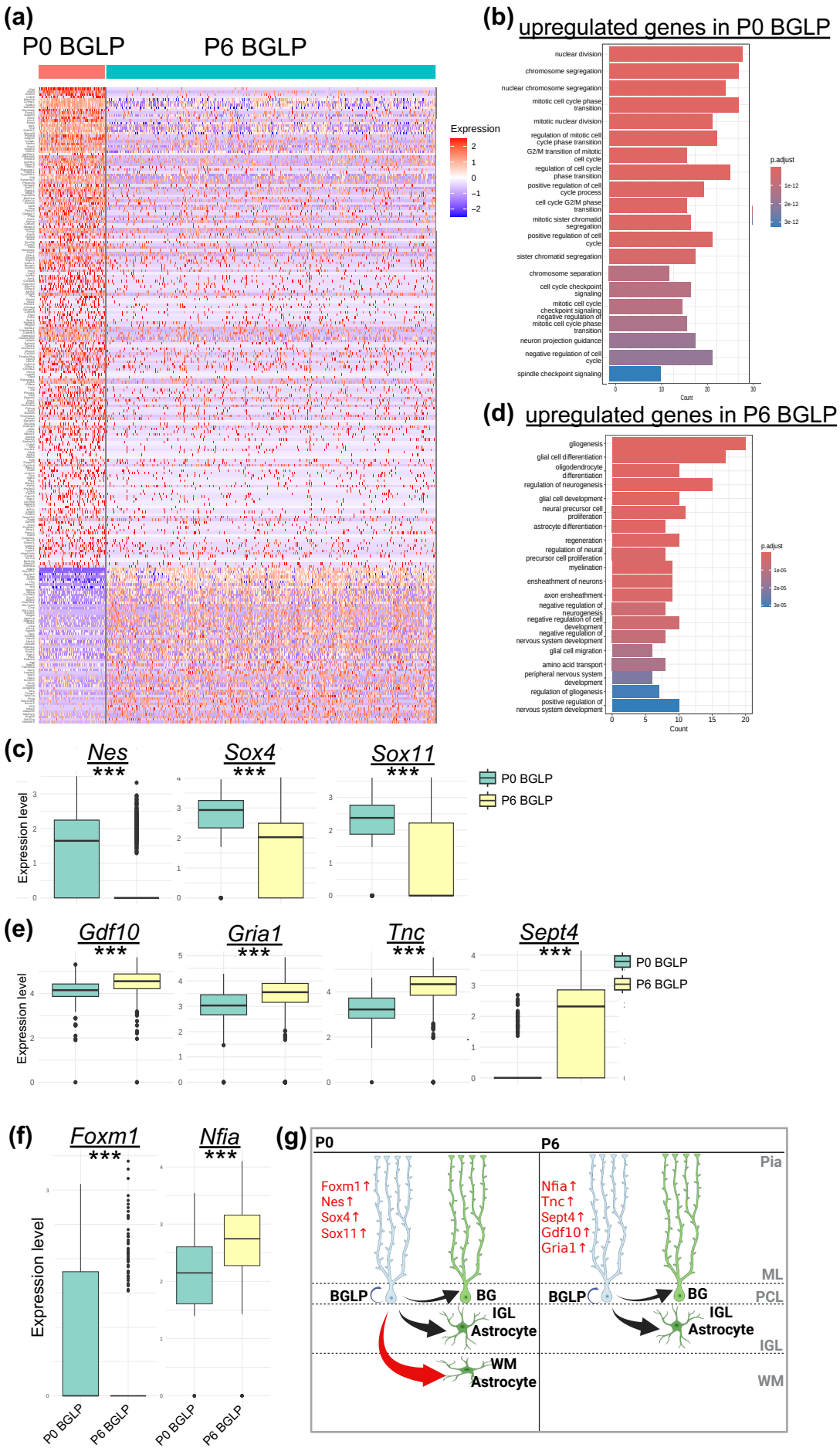

Fig8. P0 mouse BGLPs show higher stem cell marker expression, while P6 mouse BGLPs exhibit elevated BG-like cell specific gene levels

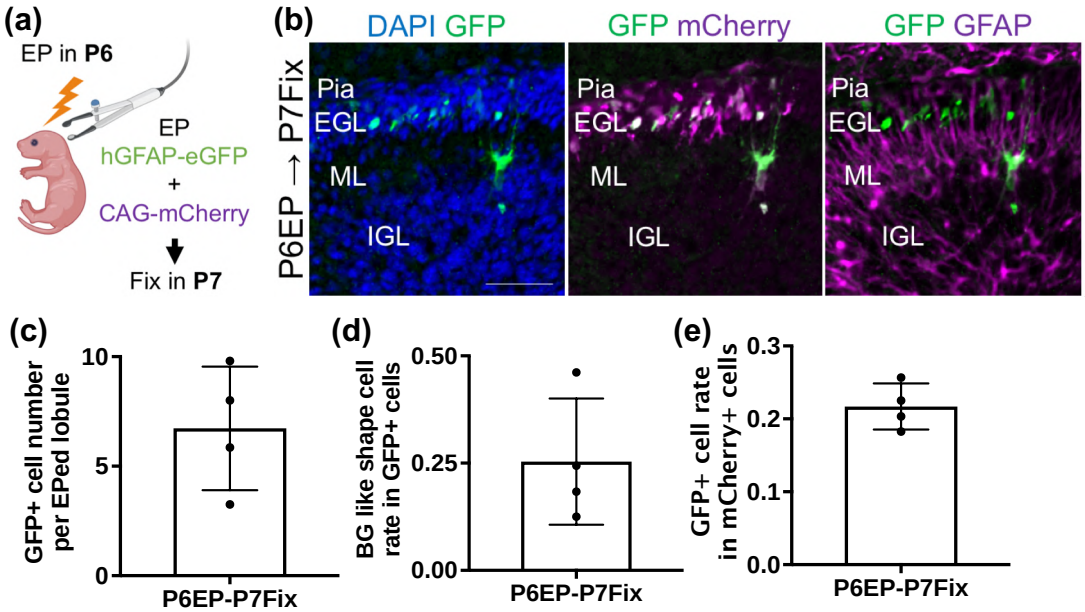

SupFig1. Results of electroporation to P6 mouse cerebellar surface with hGFAP-promoter

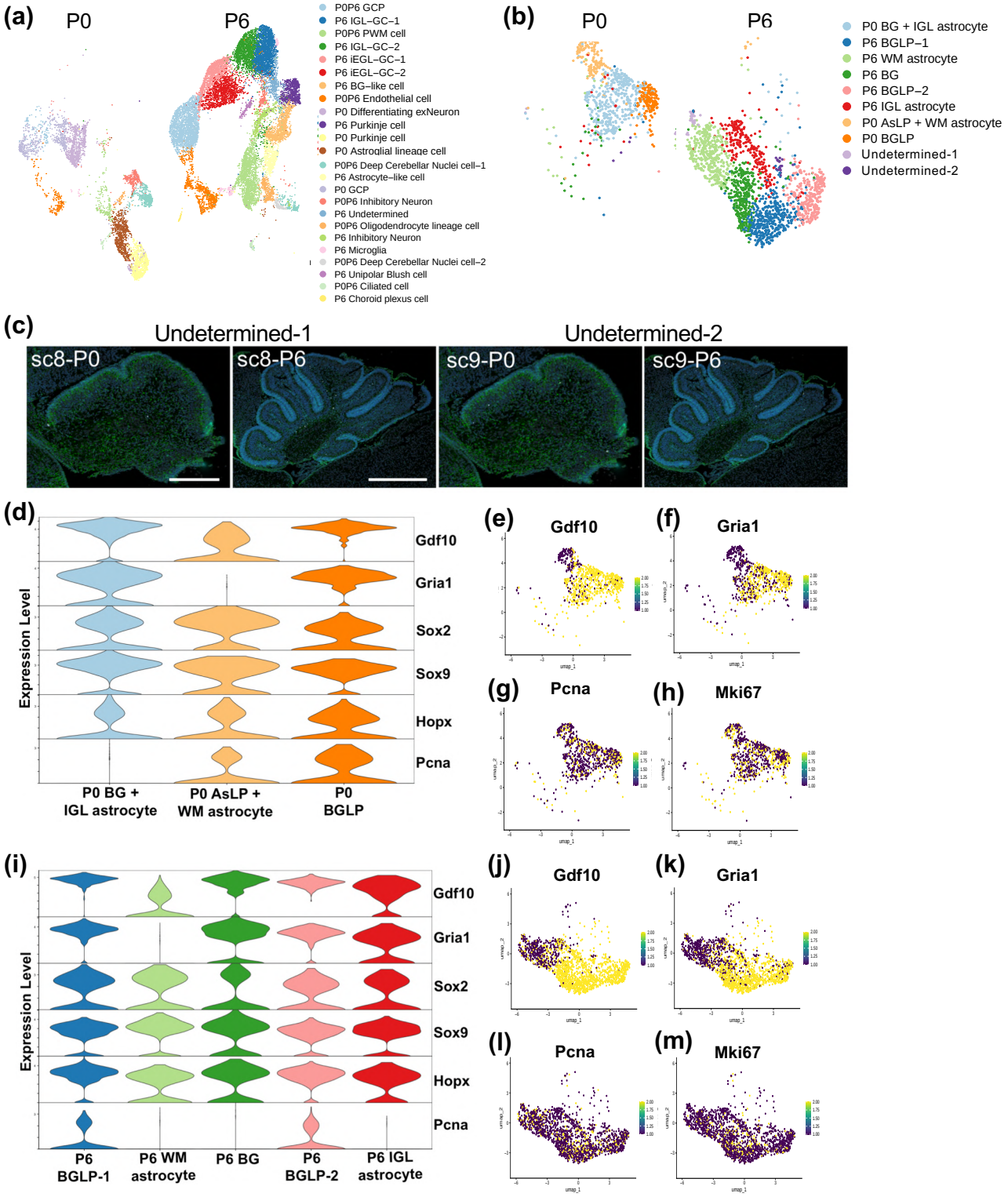

SupFig2. Supplemental data for Figure 7

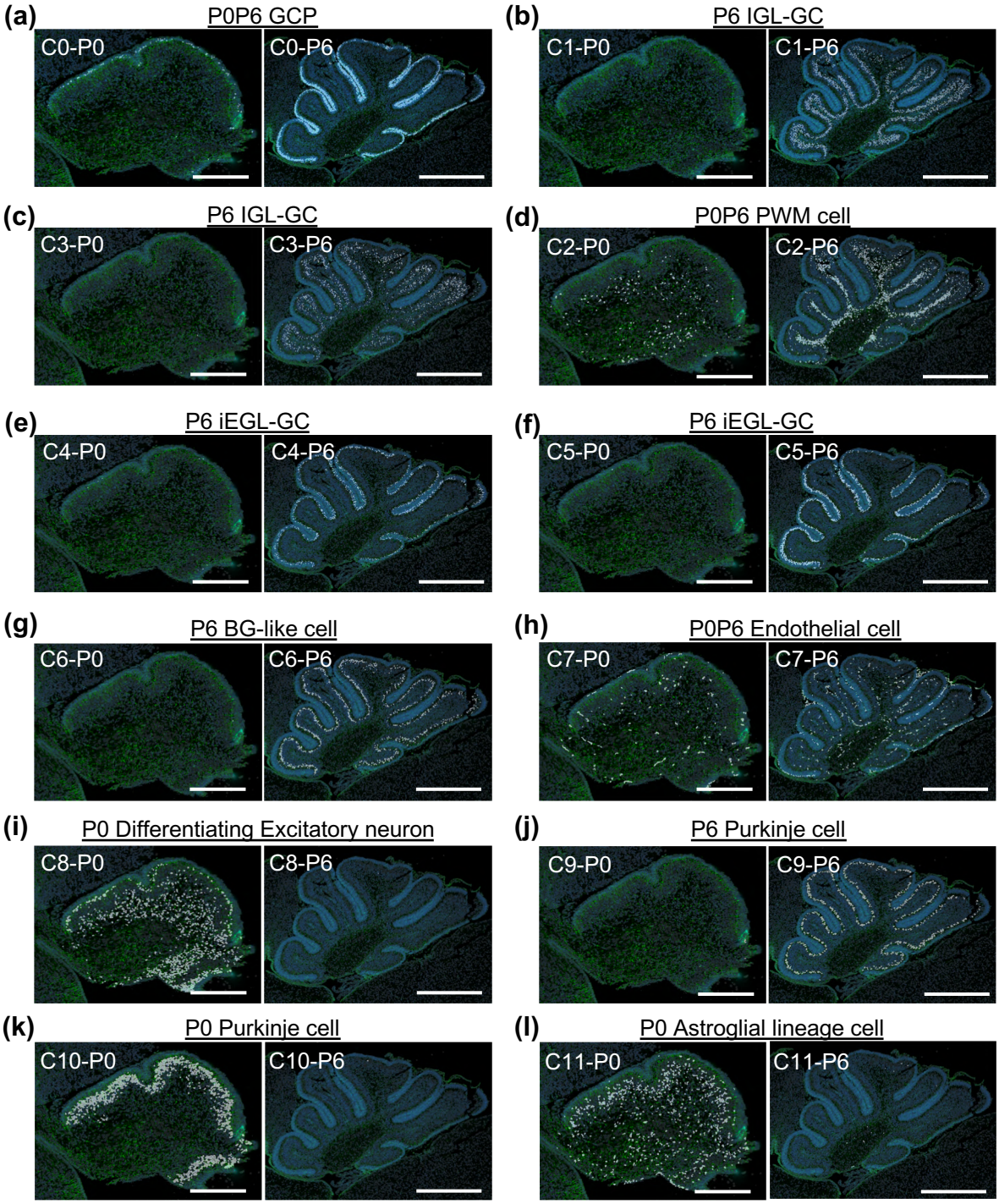

SupFig3. Spatial information of each 24 cluster

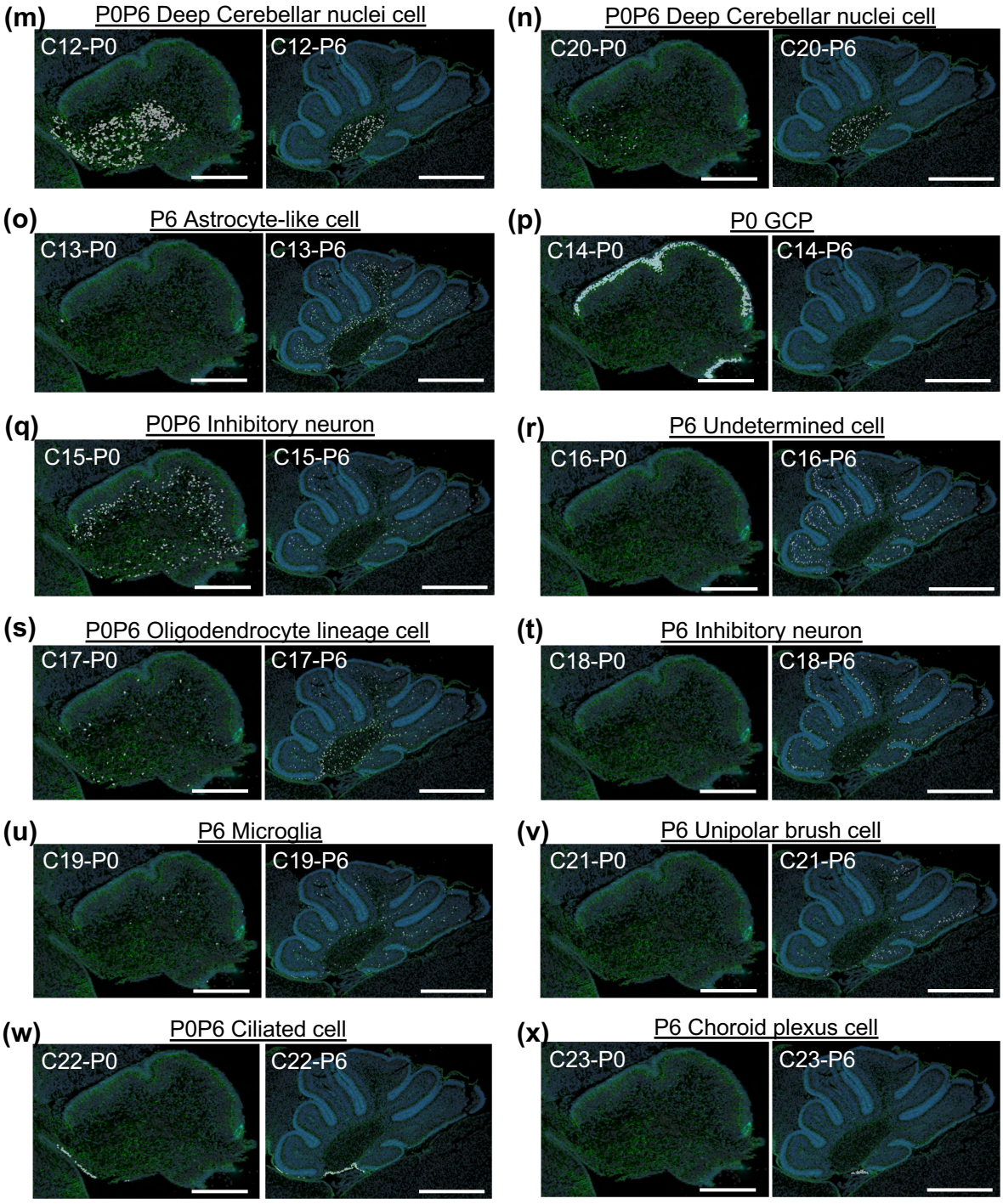

(Continue) SupFig3. Spatial information of each 24 cluster